

Least Squares Discretizations (LSQD): a robust and versatile meshless paradigm for solving elliptic PDEs

Anna Kucherova^a, Gbocho M. Terasaki^a, Selma Strango^b, Maxime Theillard^a

^a*Department of Applied Mathematics, University of California, Merced, California 95343, USA.*

^b*Department of Mathematics, University of California, Davis, California 95616, USA.*

Abstract

Searching for numerical methods that combine facility and efficiency, while remaining accurate and versatile, is critical. Often, irregular geometries challenge traditional methods that rely on structured or body-fitted meshes. Meshless methods mitigate these issues but oftentimes require the weak formulation which involves defining quadrature rules over potentially intricate geometries. To overcome these challenges, we propose the Least Squares Discretization (LSQD) method. This novel approach simplifies the application of meshless methods by eliminating the need for a weak formulation and necessitates minimal numerical analysis. It offers significant advantages in terms of ease of implementation and adaptability to complex geometries. In this paper, we demonstrate the efficacy of the LSQD method in solving elliptic partial differential equations for a variety of boundary conditions, geometries, and data layouts. We monitor h-P convergence across these parameters/settings and construct an *a posteriori* built-in error estimator to establish our method as a robust and accessible numerical alternative.

Keywords: meshless, least squares, h-P convergence, arbitrary geometries, complex boundary conditions

1. Introduction

In the ever-evolving landscape of computational science and engineering, the quest for accurate, efficient, and versatile numerical methods remains paramount. Traditional numerical approaches, such as finite element methods, finite difference methods, and finite volume methods, have long dominated the sphere of simulating complex physical phenomena. However, their reliance on elements, structured grids, or finite volumes often presents challenges when handling irregular geometries, dynamic domains, or intricate boundary conditions. In response to these limitations, a trailblazing paradigm emerged: meshless methods [18, 35].

Gaining traction almost two decades post-emergence [1, 2, 4, 5, 27, 34], meshless methods have witnessed a surge in popularity across a multitude of disciplines, including computational fluid dynamics, structural mechanics, electromagnetics, and biomedical engineering [39, 31, 22, 26]. Their inherent attributes (*e.g.* mesh generation simplicity, capacity to handle large deformations/distortions and complex geometries [32], etc.), have proven a versatile alternative to the traditional discretization techniques.

Some of the pioneering meshless methods fall into the following categories: kernel-based [18, 34, 57], Galerkin [4, 6, 12, 1, 54, 2, 19, 56, 20, 10, 3], and Finite Difference methods [33, 42]. Meshless Galerkin methods such as the Element-free Galerkin [4, 6], h-p clouds and h-p methods [12], Meshless Local Petrov-Galerkin [1, 2], the Natural Element Method [54, 19, 56], the Voronoi finite volume method [20, 10], and partition of unity method [3], all rely on the weak formulation of the partial differential equation (PDE). Thus, although they are meshless, these methods are not truly “geometry-free” as the weak formulation involves spatial integrals. This requires approximations of definite integrals, or quadrature rules, over - potentially - intricate geometries. These geometries, themselves, may reap extravagant computational costs (*e.g.* Voronoi partition for the Meshless Natural Element method [54, 19, 56] or any Voronoi Finite

*Corresponding author: mtheillard@ucmerced.edu

Volume Method [20, 10]). Undeniably, the theoretical foundation for the aforementioned methods allows for a comprehensive mathematical study but may serve as a deterrent for interested non-experts. Clearly, it would be a quixotic undertaking to create an encyclopedic inventory for the trajectory of all meshless methods, so for an exhaustive analysis, we direct interested readers to the following reviews [41, 44, 13].

Although commonly used in scattered data interpolation [15], Kansa became one of the first to utilize radial basis functions (RBF) to solve fluid dynamics problems [27]. Theoretical condition number estimates indicated that some meshless methods using RBFs may be unstable [11]. Fortunately, Kansa was able to successfully circumvent the ill-conditioned system by using improved multi-quadrics and adaptive techniques [28]. Kansa’s method represents the solution as a sum of global radial functions, centered at a set of points. The coefficients in this decomposition are obtained by interpolating the PDE at these points. While in general, the interpolation system can be ill-posed (Mairhuber-Curtis theorem [38, 9]), when using appropriate radial functions, this system can be proven to be non-singular [40, 46]. Not solely is it straightforward to implement, this method is particularly well-suited for problems involving complex curved surfaces (*e.g.* such as reaction-diffusion patterns over biological entities such as frog species [45], red blood cells [16], or 3-D spherical shells [55] used in geophysical calculations). It has since been applied in the computational fluid dynamics realm [48] such as the solution of Navier–Stokes equations [36], porous media flow [49], and the solution of solid-liquid phase change problems [29]. Unfortunately, the convergence of Kansa’s method is still unproven. Because the representation is global, the interpolation system is full and consequently its inversion rapidly becomes prohibitive. To address this limitation, domain decomposition techniques can be employed [37], but these abandon the meshless nature of the domain. Using local RBFs [21], the local Kansa method [49, 50] offers an alternative approach to reduce the complexity. However, this approach still relies on a domain decomposition to distinguish between inner and border nodes, further requiring functional iterations on either node sets.

One of the most pervasive methods in computational fluid dynamics is the finite point method - a mesh-free method for solving PDEs on scattered distributions of points. This method is considered a generalization of the finite difference method, created for arbitrary irregular grids [33, 8]. Despite the fact that this method requires a much lower mathematical background, it entails a more tedious implementation as the discretization coefficients are obtained from high-order Taylor expansions over non-uniform neighborhoods [42]. With the Radial Basis Function Finite Difference (RBF-FD [14]), these coefficients are computed at each point by interpolating the solution over a small neighborhood using a radial basis enriched with polynomial functions. The RBF ensures good conditioning while the polynomial enrichment grants convergence. The radial basis function-based differential quadrature approach (RBF-DQ [52]) proposes a similar strategy and has been employed to simulate compressible flows [52] and heat conduction [53] problems.

Despite offering significant advantages (*e.g.* flexibility in handling complex geometries, avoiding computational overhead associated with mesh generation), meshless methods possess considerable limitations. One notable limitation is that most meshless methods must use background cells to integrate a weak form over the entire problem domain. The requirement of background cells for integration makes the method not “truly” meshless. Another challenge lies in enforcing boundary conditions accurately, especially so, as the degree of freedom may not be adapted to the problem geometry. As pointed out by Atluri and Zhu, in their work on meshless local Petrov-Galerkin methods, ensuring the satisfaction of boundary conditions in meshless methods can be non-trivial, potentially leading to inaccuracies in the solution; they attempt to mitigate this by implementing a penalty function [1]. Additionally, the lack of a structured mesh results in reduced convergence rates and increased computational costs; this occurs particularly in problems with high gradients or regions of varying solution behavior [4]. These limitations underscore the importance of carefully assessing the suitability of meshless methods for specific numerical analysis tasks and considering alternative approaches where appropriate.

In amalgamating the desired advantages of meshless methods: accessibility, simplicity, h-P convergence, and low complexity, while simultaneously relinquishing the need for rigorous theoretical validation, we present the Least Squares Discretization method (LSQD). This approach only assumes that around each point, the solution can be decomposed on a local basis. No weak formulation of the PDE, nor numerical analysis theory is needed to discretize the problem. Instead, the PDE and boundary conditions are pointwise evaluated, and the local expansions are connected through pointwise continuity conditions. All of these conditions are expressed as linear equations involving evaluations of the known local basis functions and

the unknown decomposition coefficients. They are regrouped in a rectangular linear system, from which the vector of unknown coefficients is defined as the least squares solution. The method is therefore entirely meshfree, requires minimal mathematical and programming background, and scales with the number of grid points.

Our computational exploration demonstrates how this method can be easily implemented to approximate solutions of elliptic PDEs completed with arbitrary boundary conditions enforced on non-trivial geometries, and using advanced data structures. We observe the solution converging both as the spatial resolution and the maximum polynomial order increase (h-P convergence), on both uniform and arbitrary highly non-graded tree structures. Because our method is meshless in nature, the underlying set of points can be chosen as virtually anything. In particular, the points do not have to conform to the problem geometry or be aligned in any specific pattern. This facilitates the construction and manipulation of the data structure and offers unbounded solution adaptivity and error control strategies.

This manuscript is organized as follows. In section 2, we present the LSQD method in the general context and discuss its practical implementation. The method is illustrated with a simple one-dimensional example. In section 3 we discuss the extension of the method to higher dimensions and propose an implementation on non-graded quadtree grids. Convergence results are provided in section 4 for a variety of grid and boundary configurations. We conclude in section 5.

2. The LSQD Method

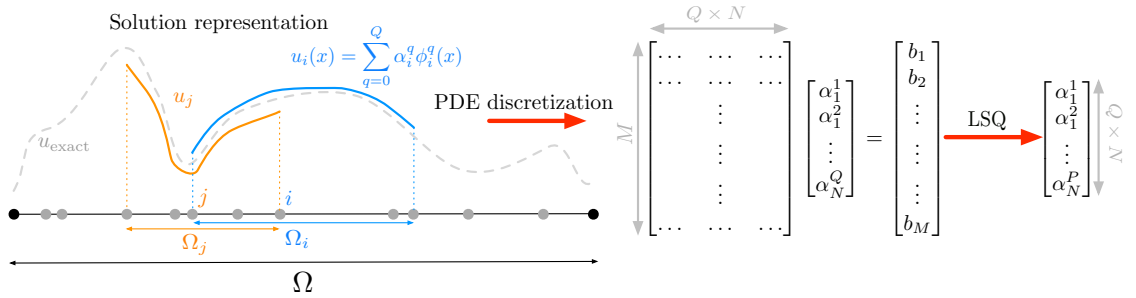


Figure 1: We represent the solution of a differential equation as a set of local expansions, denoted by $u_i(x)$, which are centered at arbitrary positions $x_{i=1..N}$. We build an overdetermined linear system by evaluating the differential equation around each neighborhood and enforcing continuity conditions between neighboring local representations. The coefficients α_i^q are the least squares solution to the overdetermined system.

2.1. General Presentation

For the LSQD method, we begin by considering the following elliptic problem:

$$au - \mu \Delta u = f(\mathbf{x}) \quad \forall \mathbf{x} \in \Omega \subseteq \mathbb{R}^d, \quad f(\mathbf{x}) \in \mathcal{C}^0(\Omega) \quad (1)$$

with generalized (e.g. Dirichlet, Neumann, Robin, etc.)¹ boundary conditions on the contour $\partial\Omega$, i.e.

$$\beta u(\mathbf{x}) + \gamma \nabla u(\mathbf{x}) \cdot \mathbf{n} = g(\mathbf{x}), \quad \forall \mathbf{x} \in \partial\Omega, \quad g(\mathbf{x}) \in \mathcal{C}^0(\Omega), \quad (2)$$

where \mathbf{n} is the outward point normal to $\partial\Omega$. The parameters of the elliptic problem, a and μ , are positive and the solution is assumed to be continuously differentiable. We are interested in constructing a discrete approximation of the solution $u(\mathbf{x})$, using a set of points $(\mathbf{x}_1, \dots, \mathbf{x}_N) \in \Omega$. To each point \mathbf{x}_i , we associate

¹For Dirichlet boundary conditions: $\gamma = 0$. For Neumann boundary conditions: $\beta = 0$. For Robin boundary conditions: $\beta \neq 0$ and $\gamma \neq 0$.

a set of neighbors V_i and define the vicinity Ω_i as the convex hull of this set. For each vicinity Ω_i , we approximate the solution using an expansion over a local smooth basis $(\phi_i^1(\mathbf{x}), \dots, \phi_i^Q(\mathbf{x}))$

$$u(\mathbf{x}) \approx \sum_{q=1}^Q \alpha_i^q \phi_i^q(\mathbf{x}), \quad \forall \mathbf{x} \in \Omega_i. \quad (3)$$

Thus, by estimating the coefficients α_i^p , at each Ω_i , we hope to construct a family of local approximations to the solution $u(\mathbf{x})$.

To find the coefficients α_i^p we evaluate the PDE (1), the continuity conditions (for \mathbf{u} and its first order derivatives), and the boundary condition (2) for the above local representation. For each node \mathbf{x}_i , we consider each neighbor pair $(\mathbf{x}_i, \mathbf{x}_j)$ with $\mathbf{x}_j \in V_i$ and construct the linear equations for α_i^p using the following procedure with three main steps:

1. **Partial Differential Equation:** we choose a point $\mathbf{x}_{ij}^{PDE} \in \Omega_i$ at which we evaluate the PDE for the expansion (3).

$$a \sum_{q=1}^Q \alpha_i^q \phi_i^q(\mathbf{x}_{ij}^{PDE}) - \mu \sum_{q=1}^Q \alpha_i^q \Delta \phi_i^q(\mathbf{x}_{ij}^{PDE}) = f(\mathbf{x}_{ij}^{PDE}). \quad (4)$$

2. **Continuity conditions:** we choose a point $\mathbf{x}_{ij}^C \in \Omega_i$ at which we enforce that the expansions centered at \mathbf{x}_i and \mathbf{x}_j are identical

$$\sum_{q=1}^Q \alpha_i^q \phi_i^q(\mathbf{x}_{ij}^C) = \sum_{q=1}^Q \alpha_j^q \phi_j^q(\mathbf{x}_{ij}^C), \quad (5)$$

and that the expansions for all first-order derivatives ∂_d are also identical at that point

$$\sum_{q=1}^Q \alpha_i^q \partial_d \phi_i^q(\mathbf{x}_{ij}^C) = \sum_{q=1}^Q \alpha_j^q \partial_d \phi_j^q(\mathbf{x}_{ij}^C). \quad (6)$$

3. **Boundary conditions:** if \mathbf{x}_i is close to the contour $\partial\Omega$, we find a point $\mathbf{x}_i^{BC} \in \partial\Omega$, at which we enforce the boundary condition for the local expansion (3).

$$\beta \sum_{q=1}^Q \alpha_i^q \phi_i^q(\mathbf{x}_i^{BC}) + \gamma \sum_{q=1}^Q \alpha_i^q \nabla \phi_i^q(\mathbf{x}_i^{BC}) \cdot \mathbf{n} = g(\mathbf{x}_i^{BC}). \quad (7)$$

Grouping all these equations, we form a rectangular system of width $Q \times N$ and height M (the total number of equations).

$$\begin{bmatrix} \dots & \dots & \dots \\ \dots & \dots & \dots \\ & \vdots & \\ & \vdots & \\ & \vdots & \\ \dots & \dots & \dots \end{bmatrix} \begin{bmatrix} \alpha_1^1 \\ \alpha_1^2 \\ \vdots \\ \alpha_N^Q \end{bmatrix} = \begin{bmatrix} b_1 \\ b_2 \\ \vdots \\ \vdots \\ \vdots \\ b_M \end{bmatrix} \Leftrightarrow A\alpha = b. \quad (8)$$

If the matrix A is full rank, we construct the coefficient vector α as the least squares solution:

$$\alpha = \underset{x}{\operatorname{argmin}} \|Ax - b\|_2 \Leftrightarrow A^T A \alpha = A^T b. \quad (9)$$

If the matrix is not full-rank, we can consider the stabilized problem

$$(A^T A + \epsilon I) \alpha = A^T b, \quad (10)$$

which is well-known to be invertible for any $\epsilon > 0$. Nevertheless, we must be cognizant of two extremities: choosing a large ϵ will affect the accuracy of the method, but choosing its value to be too small may leave the system singular to machine precision. We address this topic in section 3.5.

2.2. Practical Implementation

2.2.1. Basis Selection

Formally, the method does not impose any restriction on the basis selection, yet, it is well known that a naive choice could lead to singular least squares systems, making it impossible to construct the solution (without stabilization). For example, allow us to consider the standard interpolation problem (*i.e.* choosing $\alpha = 1$ and $\mu = 0$ in (1), with appropriate boundary conditions); from the Mairhuber–Curtis theorem [38], we know that choosing global non-centered basis functions may result in a singular interpolation matrix. For the rest of this study, at each point \mathbf{x}_i we will use polynomial functions, centered at the point \mathbf{x}_i and rescaled by the size of the neighborhood V_i . In doing so, we aim to limit singularities in the final least squares system, as well as provide a framework for achieving high-order convergence. We will denote by P the maximum polynomial order of the basis, and continue to denote by Q , the total number of elements in the basis.

2.2.2. Neighborhood Construction

From the method description, we see that it is important to construct a full-rank matrix A , while trying to keep it as compact and sparse as possible for computational efficiency. The matrix structure and size are primarily dictated by the neighborhoods configurations. It is therefore imperative to understand how many neighbors are needed in each neighborhood, how to construct them, and what properties they should satisfy. In particular, we identify three key properties the neighborhood must satisfy

- i **System Size** - The total number of equations must be greater or equal to the total number of basis functions (*i.e.* the number of unknown coefficients).
- ii **Connectivity** - The neighbors' adjacency matrix must be invertible, or in other words the neighboring graph must be irreducible. In practice, it means that traveling along neighboring connection, you should be able to travel from any point \mathbf{x}_i to any other point \mathbf{x}_j .
- iii **Independence** - The neighborhood should contain points with at least $P + 1$ unique coordinates in each directions.

The first condition is necessary for the matrix A to be full rank. The second condition ensures that all the neighborhoods are connected, and therefore, that the computation of each basis's coefficients depends on all other coefficients. If this condition is not satisfied, there will be clusters of nodes and, consequently, basis coefficients that are separated from each other, violating the global nature of the elliptic equation (1). The third condition reinforces linear independence between the coefficient equations. It is constructed from the observation that if the problem is invariant in all directions except one, the matrix A must still be full rank. In that case, the number of linearly independent basis functions is simply $P + 1$ and so we need at least as many unique coordinates in the non-invariant direction.

We point out that the neighborhoods do not have to be symmetric, meaning that if \mathbf{x}_j is a neighbor of \mathbf{x}_i (*i.e.* $\mathbf{x}_j \in V_i$), \mathbf{x}_i does not have to be a neighbor of \mathbf{x}_j . They do not all have to be the same size, nor respect specific geometric configurations. In practice though, it is natural to keep them local and compact.

2.2.3. Evaluation Points

As mentioned in 2.1, the evaluation points \mathbf{x}_{ij}^{PDE} and \mathbf{x}_{ij}^C for the PDE and continuity conditions must be chosen in the domain Ω_i where the local i^{th} expansion is formally defined. Typically, the evaluation points are selected to be on the line segment $[\mathbf{x}_i, \mathbf{x}_j]$ as this ensures locality. We note that choosing different evaluation points for the PDE and continuity conditions ($\mathbf{x}_{ij}^{PDE} \neq \mathbf{x}_{ij}^C$) may reinforce linear independence.

The boundary conditions are only evaluated when the point \mathbf{x}_i is close to the interface $\partial\Omega$. As well as other method parameters, *proximity of the interface* must be defined in each context. For example, in 1D, we can place boundary points on the interface and evaluate the boundary condition at these points only. In higher dimension, provided that we have a smooth implicit representation (e.g. a level-set representation), we can always detect whether Ω_i crosses $\partial\Omega$, and if so, find at least one point \mathbf{x}_i^{BC} on $\Omega_i \cap \partial\Omega$.

2.2.4. System Construction & Inversion

The main advantage of our method is that the matrix A is straightforward to construct. Once the neighborhoods have been constructed, we need to loop over all neighboring pairs and evaluate the PDE, continuity, and boundary conditions. The matrix assembly only requires evaluation of the basis function at the evaluation points. No quadrature rule, finite difference formula, or any other numerical analysis algorithms are required.

Assuming that the Least Squares problem is non-singular, the solution vector can be computed using a preconditioned conjugate gradient method (since $A^T A$ is symmetric), or using the LSQR method [43, 51] to avoid forming $A^T A$. Forming $A^T A$ may allow us to construct a wider range of preconditioners, and so it is, *a priori*, unclear which of these options will be computationally more efficient. It should be noted that the matrices A , A^T , and $A^T A$ are sparse and can be constructed in $\mathcal{O}(NQ^2)$ and $\mathcal{O}(NQ^3)$ respectively. Therefore, leaving aside the neighborhood construction, the total computational cost will scale as the complexity of the linear solver, typically $\mathcal{O}(NQ^3\sqrt{\kappa})$, with κ being the condition number of $A^T A$.

2.3. One-Dimensional Illustration

We consider the following Poisson problem

$$\begin{aligned} -\Delta u &= f(x) & \forall x \in \Omega = [0, 1], \\ u(x) &= g(x) & \forall x \in \partial\Omega. \end{aligned} \tag{11}$$

In order to study the performance of the method we choose the exact solution to be

$$u_{\text{exact}}(x) = \sin(7x) + \cos(7x)$$

and we set $f(x)$ and $g(x)$ accordingly. All local basis function sets are chosen to be centered and rescaled polynomials, *i.e.* for each x_i and over each corresponding neighborhood V_i , we define

$$\phi_i^q(x_i) = \left(\frac{x - x_i}{|V_i|} \right)^{q-1}, \quad |V_i| = \max_{j \in V_i} |x_i - x|, \quad x \in V_i, \quad q = \{1, \dots, Q = P + 1\}. \tag{12}$$

Each neighborhood V_i is first created by choosing the node \mathbf{x}_i itself, its closest left and right neighbors. This ensures that the neighborhoods overlap with at least another neighborhood in each direction and therefore that the connectivity condition **ii** is satisfied. Additionally, because the cardinality of the basis set is equal to $P + 1$, we need at least $P + 1$ different neighbors in V_i to satisfy both the system size **i** and independence **iii** conditions. Therefore, if $P > 2$, we add the remaining $P - 2$ closest points to the neighborhood. As a result, each neighborhood will contain $\eta = \max(3, P + 1)$ elements. For simplicity, we choose the evaluation points to be $\mathbf{x}_{ij}^{PDE} = \mathbf{x}_{ij}^C = \mathbf{x}_j$.

Once again, we emphasize the fact that advanced numerical analysis techniques are not required to construct our system, nor to obtain our solution (e.g. no Taylor expansions, convoluted integrals, or quadrature rules). Our implementation contains around 100 lines of MATLAB code and the least squares system is solved using the simple backslash solve command (*i.e.* $\alpha = A^T A \backslash A^T b$). The backslash command for general square matrices uses LU decomposition; however, for symmetric matrices (which is our case) the Cholesky decomposition is used instead. The results can be seen in Figure 2.

To study the h-P convergence of the method, we initialize the points $x_{i=1..10}$ at random and then recursively add midpoints between adjacent neighbors to double the local spatial resolution. We will refer to splits as the number of subdivisions performed from the original points set, and point out that the local resolution scales like $h^{-\text{splits}}$, where h is the original local spatial resolution. In parallel, we vary the polynomial order using $P = 2, 3, 4$. The error is computed by comparing the exact solution and the local approximation at each point. We will focus on the maximum error only.

Convergence results are compiled in Figure 3, where we see the error diminishing both as the resolution and the polynomial order increase. On the other hand, the condition number inflates with both the resolution and maximum polynomial order; this phenomenon should be seen as a proxy for the computational time needed to solve the least squares problem. This is as one might expect and is the exchange we are willing to make in the name of simplicity for this method.

With the system being symmetric, we can precondition it using a standard incomplete Cholesky decomposition, which, for this example, drastically reduces the condition number. Typically, the condition number of the preconditioned system is the square root of the unpreconditioned one. As we will see in section 4.6 the discontinuities between adjacent expansions can be used to estimate.

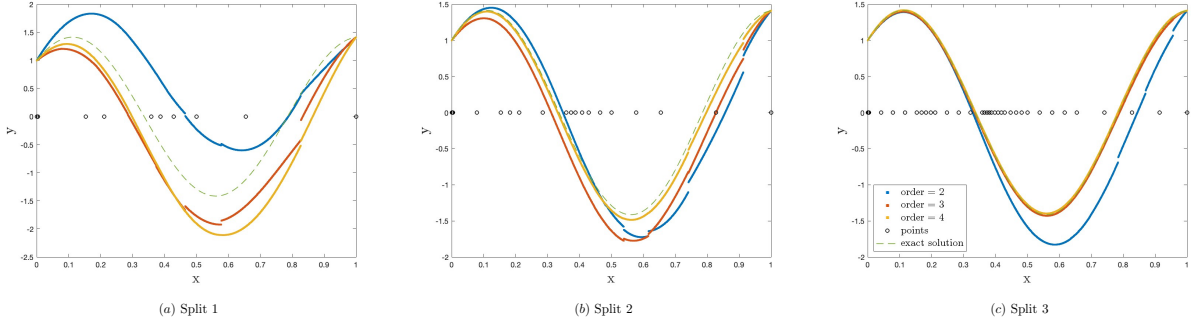


Figure 2: 1D Method - solution representation for increasing spatial and polynomial resolution. We start from a randomly generated set of points $\mathbf{x}_{i=1..10}$ and then recursively split the grid by adding one grid point exactly between each existing pair of direct neighbors. The exact solution is depicted in dashed lines.

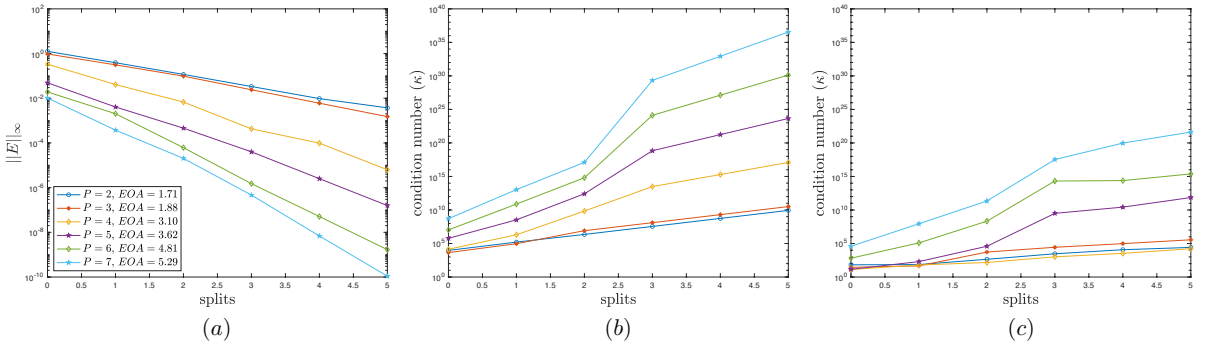


Figure 3: 1D Method - (a) h-P convergence analysis for Poisson's equation with Dirichlet boundary conditions. L^∞ error and corresponding Estimated Order of Accuracy (EOA). (b) Condition number of the least squares matrix $A^T A$. (c) Condition number of the preconditioned least squares matrix, using an incomplete Cholesky decomposition.

3. Extension to Higher Dimensions & Implementation on Quadtree Grids

Despite the one-dimensional example serving as an obligatory proof of concept in terms of convergence, the full capabilities of our method, such as dealing with highly adaptive data structure and arbitrary geometries and boundary conditions, only manifest themselves in higher dimensions.

For our method, the extension to higher dimensions is straightforward from both the theoretical and practical perspectives. As illustrated in Figure 4, the domain of interest Ω is still discretized by a set of points $\mathbf{x}_{i=1..N}$. The solution is then decomposed over a local basis $\phi_i^1(\mathbf{x}).. \phi_i^Q(\mathbf{x})$ around the set of points, and the coefficients for these expansions are obtained by evaluating the partial differential equations, boundary, and continuity conditions over local neighborhoods, as underscored in section 2.1. The construction of the linear system remains unambiguous and the properties of the final system are unchanged ($A^T A$ is symmetric, positive definite).

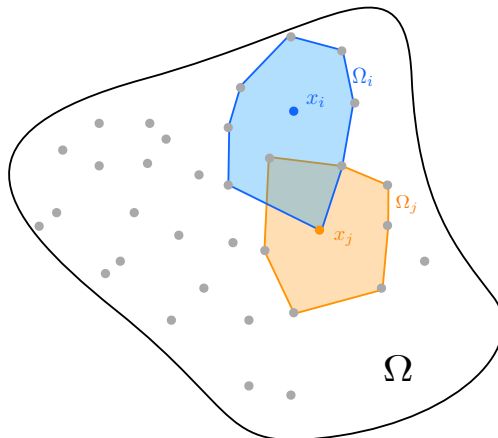


Figure 4: Extension to higher dimensions: domain of interest Ω , and local vicinities Ω_i, Ω_j . The neighborhoods V_i, V_j are defined as the set of points contained in the corresponding vicinities.

The main difference lies in the neighborhood construction: both in their shape and size. In 1D, finding close neighbors from a pre-sorted list is trivial. In higher dimensions, for an efficient construction, the pre-sorting must be done using more complex data structures, such as sorting trees or hash tables.

Also, because the derivative continuity condition will be evaluated in each direction, the total number of equation written per neighboring pair will differ, and thus the minimal neighborhood size. Namely, in d -dimensions, for a neighborhood V_i composed of η neighbors (including \mathbf{x}_i), we will evaluate

- η PDE equations,
- $\eta - 1$ continuity conditions,
- $d(\eta - 1)$ first-order derivative continuity conditions ($\eta - 1$ for each partial derivative),

so a total of $\eta(d + 2) - d - 1$ equations. Since we want the matrix A to be full rank, we will systematically pick the number of basis of local basis function Q such that

$$Q \leq \eta(d + 2) - d - 1. \quad (13)$$

Note that this strategy does not account for the boundary condition evaluations. This is an intentional decision to derive a robust and simple strategy: the total number of boundary condition evaluations is hard to predict *a priori*, and these conditions will only increase the system size and rank.

Since sorting structures will be needed to construct neighborhoods, we will locate the points at the cell centers of a Quadtree to limit the number of data structures and facilitate the presentation and implementation of our method. Quadtree grids [47], a paradigmatic data structure for high-performance computations (see *e.g.* [30, 7, 17, 23]). The points \mathbf{x}_i will be located at the tree's cell centers. We will represent the domain Ω through a level-set function and only approximate the solution at the points located inside Ω (see Figure 6).

3.1. 2D Basis Functions

We chose our basis functions as products of one-dimensional rescaled polynomials. Namely around $\mathbf{x}_i = (x_i, y_i)$:

$$\phi_i^q(\mathbf{x}) = \left(\frac{x - x_i}{|V_i^x|} \right)^{p_x} \left(\frac{y - y_i}{|V_i^y|} \right)^{p_y} \quad \forall \mathbf{x} = (x, y) \in \Omega_i, \quad (14)$$

where the rescaling coefficients are

$$|V_i^x| = \max_{\mathbf{x} \in V_i} |x_i - x|, \quad |V_i^y| = \max_{\mathbf{y} \in V_i} |y_i - y|. \quad (15)$$

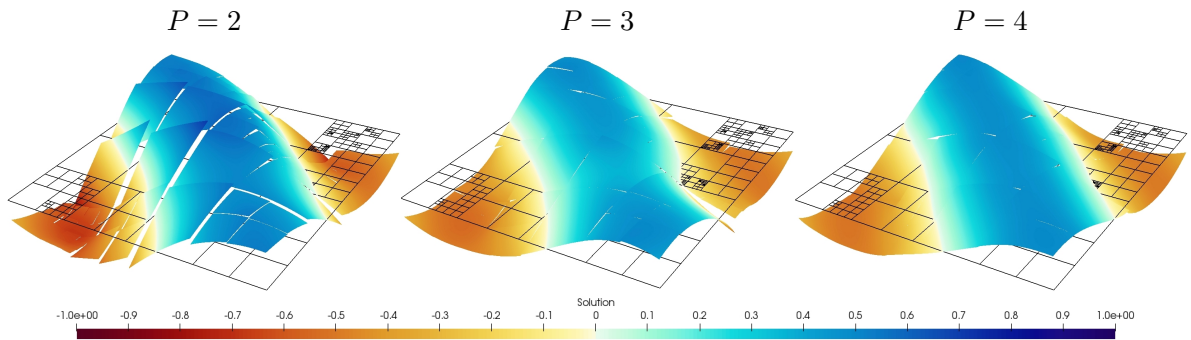


Figure 5: LSQD Approximation of the function $u_{\text{exact}} = \cos(x + y)$ for increasing polynomial order on an arbitrary Quadtree grid.

The rescaling helps keep the coefficients in A – therefore of $A^T A$ – of similar magnitude, consequently keeping the condition number of $A^T A$ low. In this context, this is essential as we are dealing with very disparate length scales and potentially high-order polynomial functions.

We consider the set of polynomial functions of degree P , meaning that $p_x + p_y \leq P$ (see Figure 5). The total number of basis functions will be

$$Q = \frac{(P+1)(P+2)}{2}, \quad (16)$$

and so conditions (13) dictates that we will need to choose the neighborhood size η such that

$$\eta \geq \frac{(P+1)(P+2) + 6}{8}. \quad (17)$$

Consider, for example, using a polynomial order $P = 7$, from the above condition we see that $\eta \geq 9$. The neighborhood will grow with the number of basis functions and, thus, local unknown coefficients. However, this growth will occur slowly, implying that the neighborhood will remain very compact; this attribute is highly desirable, especially in higher dimensions, as keeping “things” as local as possible implies keeping A and $A^T A$ as sparse as possible. The above inequality (17) is not enough to specify η as the connectivity (ii) and independence (iii) conditions must also be satisfied.

3.2. Tree-Based Neighborhood Construction

Figure 6 illustrates the construction of the neighborhood V_i for any given point \mathbf{x}_i . We start by adding the point itself (blue) to the neighborhood. Next, the algorithm recursively picks a direct neighbor in each direction for each point in the neighborhood and store them in a candidate set (pink). In this set, the candidates are sorted in counterclockwise order starting to the right. In case one of the candidates lies outside Ω (see bottom row of Figure 6), we move it to the ghost set G_i that will be used to find evaluation points for the boundary condition.

On the first pass, we add the entire candidate set to the neighborhood to ensure that the connectivity condition (ii) is met. On the subsequent passes, while the other two conditions are not met, we go through the candidates set and add a candidate \mathbf{c} to the neighborhood if either

- (a) The system size condition (i), reformulated as inequality (17), is not met.
- (b) The independence condition (iii) is not met in at least a direction d and the coordinate c_d of the candidate in that direction is not already present in the neighborhood, *i.e.* $\forall \mathbf{v} \in V_i \quad v_d \neq c_d$.

We point out that using non-uniform point distributions reduces repetition in the coordinates, which eases the fulfillment of condition (iii) and ultimately generates smaller and more compact neighborhoods. If the grid is refined enough, the algorithm mentioned above will always converge, which allows us to

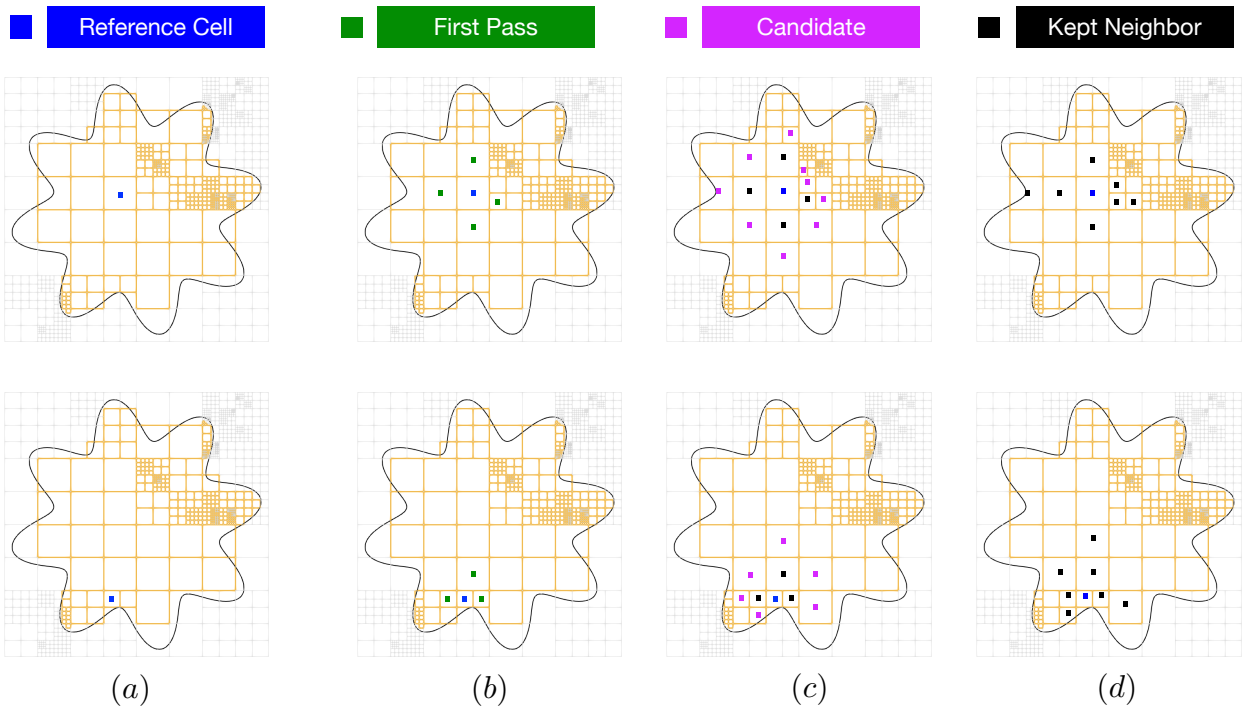


Figure 6: Illustration of neighborhood construction around a reference cell (in blue) for polynomial basis order $P = 4$. The process is carried out one layer at a time until enough neighbors are identified to satisfy the system size and independence conditions. When the reference cell lays next to the interface, the neighbors are chosen within Ω (bottom row). The solution is only constructed at the cell centers of the orange cells located inside Ω . The outside grey cells are only used to locate the interface while evaluating the boundary condition.

systematically construct neighborhoods. However, in case the grid is under-resolved, there may not be enough neighbors available, which can lead to infinite loops. To prevent this, we set a maximum number of passes (usually $P + 4$). In these degenerated situations, the grid is inconsistent with the polynomial order and geometry, so the problem is completely under-resolved, and the method will produce an inaccurate solution. In the next section, we will explain how we use the neighborhood to evaluate the problem and form a linear system.

3.3. Evaluation points

For simplicity, we keep the continuity and pde evaluation points identical ($\mathbf{x}_{ij}^{PDE} = \mathbf{x}_{ij}^C = \mathbf{x}_j$). For the evaluation of the boundary condition, we go through the set of ghost neighbors G_i obtained through the neighborhood construction, and for each ghost \mathbf{g} neighbor we find a point $\mathbf{x}_{ig}^{BC} \in [\mathbf{x}_i, \mathbf{g}]$ lying on the interface and evaluate the boundary condition there. Since we are using an implicit representation for the interface (level-set), finding \mathbf{x}_{ig}^{BC} boils down to a zero-finding problem on the segment $[\mathbf{x}_i, \mathbf{g}]$ which is easily solved using, for example, the bisection method.

If \mathbf{x}_i is located at the center of a cell at the edge of the computational domain, the boundary condition is evaluated on the corresponding edges.

3.4. Matrix Rescaling

In addition to the basis function rescaling, we rescale the rows of the matrix A by their respective norms. This operation should be seen as a re-weighting of each linear equation, *i.e.* multiplying the entire system by a diagonal matrix with non-zero diagonal entries. In doing so, we keep the magnitude of the coefficients in A as close to each other as possible to ensure that the final condition number is as low as possible. Specifically,

we start by computing the weighting coefficients w_k as the inverse of the row norms of $A = (a_{kl})$

$$w_k = \left(\sum_{l=1}^{Q \times N} |a_{kl}| \right)^{-1} \quad \forall k = 1, 2, \dots, M \quad (18)$$

and then rescale the entire system

$$a_{kl} = a_{kl} w_k \quad \forall k = 1, 2, \dots, M, \quad l = 1, 2, \dots, Q \times N \quad (19)$$

$$b_k = b_k w_k \quad \forall k = 1, 2, \dots, M. \quad (20)$$

Recall M is the total number of equations in the overdetermined system.

3.5. Stabilization of the LSQ System

As discussed earlier, the final least squares system is guaranteed to be invertible if a small diagonal perturbation ϵ is added. This addition may not be necessary, especially as it essentially penalizes large coefficients, thus affecting the accuracy of the method. In practice, this stabilization should be seen as a means to keep the condition number of the system bounded.

Adding the diagonal perturbation effectively shifts the spectrum of the system. We know that the eigenvalues λ_k of $A^T A$ are positive, and so the condition number of $A^T A$ is the ratio of the largest and smallest eigenvalues λ_{\max} and λ_{\min}

$$\kappa(A^T A) = \frac{\lambda_{\max}}{\lambda_{\min}}.$$

If λ_k is an eigenvalue of $A^T A$, $\lambda_k + \epsilon$ is an eigenvalue of the stabilized problem $A^T A + \epsilon I$, and so the condition number of the stabilized problem is

$$\kappa(A^T A + \epsilon I) = \frac{\lambda_{\max} + \epsilon}{\lambda_{\min} + \epsilon}.$$

If we set a practical maximum condition number κ_M for the stabilized system, and seek the minimal perturbation needed ϵ_{\min} to remain below this limit

$$\kappa_{\max} = \frac{\lambda_{\max} + \epsilon_{\min}}{\lambda_{\min} + \epsilon_{\min}},$$

we find that

$$\epsilon_{\min} = \frac{\lambda_{\max} - \kappa_{\max} \lambda_{\min}}{\kappa_{\max} - 1}.$$

For the current implementation we set $\kappa_{\max} = 10^{40}$, and estimate the largest and smallest eigenvalues of $A^T A$ using Gershgorin circles theorem

$$\begin{aligned} \lambda_{\max} &= \max_{k=1..M} c_{kk} + \sum_{l \neq k} |c_{kl}|, \\ \lambda_{\min} &= \max \left(0, \min_{k=1..M} c_{kk} + \sum_{l \neq k} |c_{kl}| \right), \end{aligned}$$

where the c_{kl} are the coefficients of the matrix $A^T A$. In practice, we measured $\lambda_{\max} \approx 10^2$, $\lambda_{\min} = 0$, leading to $\epsilon \approx 10^{-38}$. We note that κ_{\max} is the maximum allowed condition number for the preconditioned system. In practice, we preconditioned the system with an incomplete Cholesky precondition, and so the final condition number will be much lower. Based on our one-dimensional observations, we expect the preconditioned condition number to be bounded above by $\approx 10^{20}$. Again, this is an upper limit that should be seen as the absolute worst-case scenario. For all cases presented in the following section, we find the least squares system to be invertible and construct the numerical solution using an iterative Conjugate Gradient method, typically taking $10^2 - 10^4$ iterations to converge to residuals $\|(A^T A + \epsilon_{\min} I)\alpha - A^T b\|_{\infty}$ smaller than 10^{-26} .

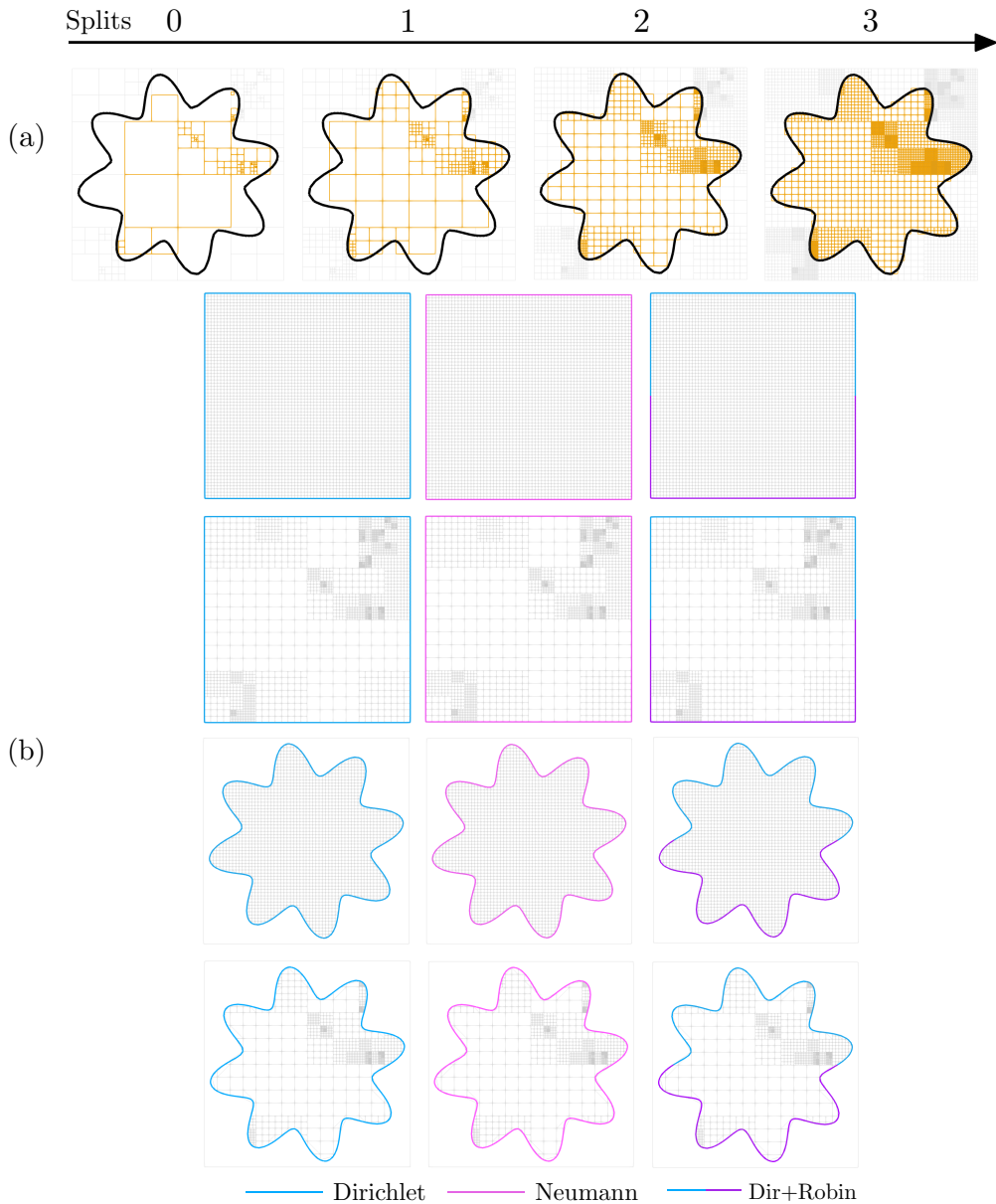


Figure 7: Configurations for the convergence analysis: (a) Illustration of arbitrary tree structures. The grid is randomly generated (first grid) which we call Split 0, then recursively refined (left to right - Split 1 to Split 3). (b) Grids and domains used - For each boundary condition type (Dirichlet, Neumann, Mixed Dirichlet Robin), enforced on a square (top rows) or the octofoil domain (bottom rows), we will consider both uniform (row 1 and 3) and adaptive grids (rows 2 and 4). This representation will be used to label all convergence figures hereafter

4. Results

Presented here are convergence results for various domain types, levels of mesh refinement, boundary condition types, and numerous formulations of equation (1) (by changing the coefficients). Furthermore, we present built-in error estimate. Finally, we discuss the implications of Neumann boundary conditions with a computational time analysis.

Table 1: Convergence summary - Average estimated order of convergence for various boundary conditions, configurations, and polynomial orders $P = 2, \dots, 5$.

	Dirichlet	Neumann	Dir.+Robin	Vary $\frac{\alpha}{\mu}$	Degenerate	Overall Avg
P = 2	1.86	2.17	2.02	1.63	1.46	1.83
P = 3	1.96	2.20	2.07	2.16	1.91	2.06
P = 4	3.45	3.30	3.46	3.51	3.45	3.43
P = 5	3.66	4.53	3.89	4.46	3.60	4.03

4.1. Problem Setup

We consider the proposed elliptic problem (1) with varying α, μ values over two domains. The first domain is the unit square $\Omega = [-1, 1] \times [-1, 1]$. The second domain is the interior of an octofoil centered at $(0, 0)$ and defined by the zero contour of the following level set equation (see Figure 7)

$$\phi(x, y) = -\left[\frac{4}{5} + \frac{4}{25} \sin\left(8 \arctan\left(\frac{y}{x}\right)\right)\right] + \sqrt{x^2 + y^2}. \quad (21)$$

For both of these domains, we use the boundary condition formulation (2) and adjust the weights β and γ to achieve the desired condition types. We also consider two types of mesh refinement: uniform and randomly generated (see Figure 7). Each of the representations will be used for the convergence analysis in section 4.

We choose the exact solution to be $u_{\text{exact}}(x, y) = e^{x+y}$ and we set the forcing term $f(\mathbf{x})$ and the boundary condition $g(\mathbf{x})$ accordingly. For each of the representations, we vary the polynomial order of our basis from 2 to 5, and recursively split all grid cells to study the h-P convergence of the L^∞ -errors (see Figure 7(a)). The local L^1 and global L^∞ -error are defined respectively as

$$\|e_u(\mathbf{x}_i)\|_1 = \left| u_{\text{exact}}(\mathbf{x}_i) - \sum_{q=1}^Q \alpha_i^q \phi_i^q(\mathbf{x}_i) \right|. \quad (22)$$

$$\|e_u\|_\infty = \max_{i=1..N} \left| u_{\text{exact}}(\mathbf{x}_i) - \sum_{q=1}^Q \alpha_i^q \phi_i^q(\mathbf{x}_i) \right|. \quad (23)$$

The Estimated Order of Convergence (EOC) will be computed from the global error, using power fitting curves.

4.2. Classical Boundary Conditions: Dirichlet, Neumann, and Robin

Consider $\alpha = \mu = 1$ for all twelve configurations presented in Figure 7. The local error convergence for the octofoil domain with a Dirichlet Boundary condition ($\beta = 1$), using an adaptive refinement is depicted on Figure 8. The h-P convergence of the global error for each set of boundary conditions is represented in Figure 9. For all twelve configurations, we see the error decaying to zero as the grid resolution and the polynomial order increase. The estimated order of convergence (see Table 1 and Figure 9) are fairly constant across all examples, ranging from approximately 2 (P=2) to 4 (P=5).

We point out that the octofoil examples on the adaptive grid, and even more so with the mixed boundary condition case (labeled "Dir. + Robin" in Figure 7), are particularly challenging to deal with traditional discretization techniques. Again, non-trivial boundary conditions are enforced on complex geometries, and the grid is randomly generated and not conforming to the interface. In fact, for these last two reasons, the traditional Finite Element Method cannot be employed here, as they require conforming mesh, and when implemented on quadtree grids, requires graded tree (*i.e.* the size ratio between neighboring cells cannot exceed 2). There are in theory no obstructions from using the Finite Differences of Volumes methods, but the constructions of the discrete differential operators and fluxes rapidly becomes a practical nightmare, especially in the high-order context. The modal Discontinuous Galerkin method allows for a systematic

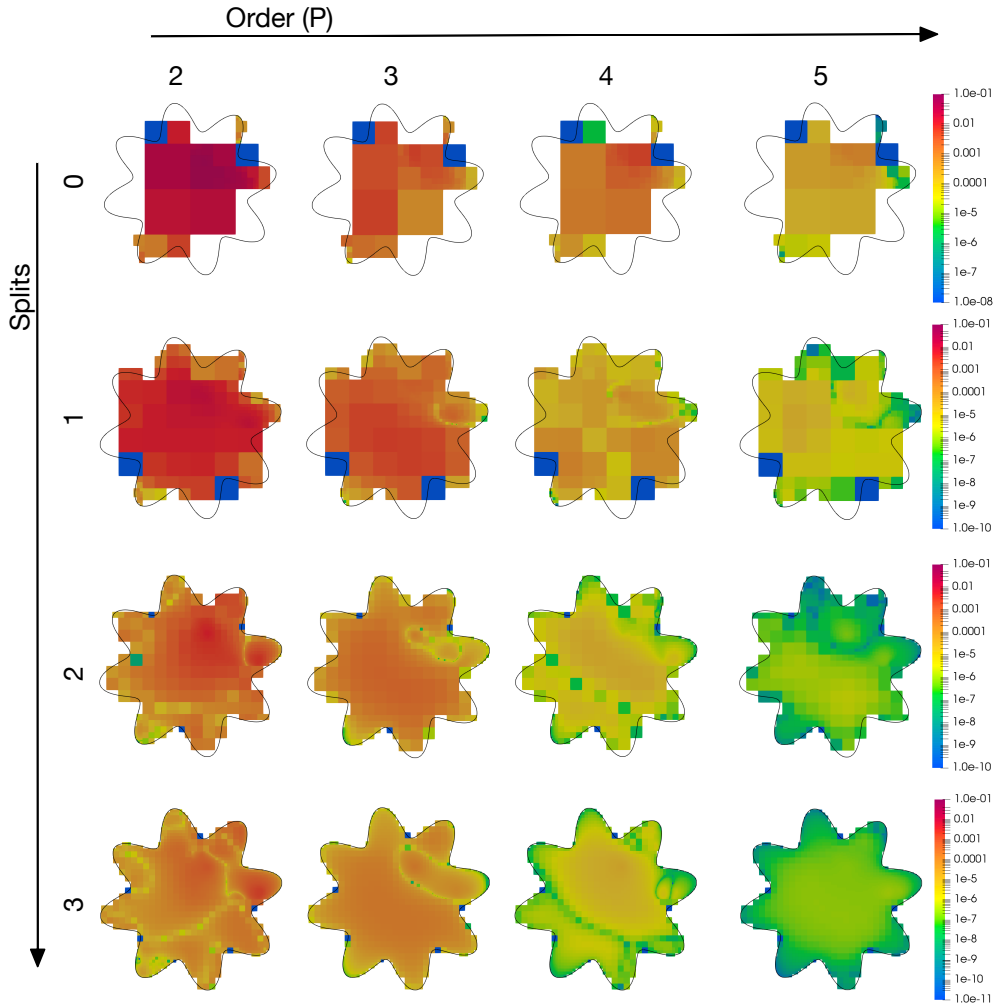


Figure 8: Convergence of the local error: Octofoil domain with Dirichlet boundary conditions and an adaptive grid. We see the error decaying to zero both as the polynomial order increases or the grid is refined.

construction of the discrete system, where volume and contour integrals must be performed on the fractions of the computational cells and faces contained in the domain of interest, which can become very involved when the mesh is not adapted to the interface. Again, LSQD requires no convoluted discretization nor quadrature formula. Even in the presence of complex data structure or geometries, simple basis functions evaluations at pre-specified locations are enough to yield above second-order convergence.

4.3. Degenerate Cases

Here, we investigate degenerate cases where the PDE or boundary conditions may lead to a non-coercive weak formulation and thus potentially ill-posed problems, non-positive or even non-invertible systems. The LSQD method obtains the polynomial coefficient from an SPD system and does not rely on the weak formulation. Similarly to the Least Square Finite Element Method (LSFEM [25, 24]), the LSQD method constructs the discrete system by evaluating the PDE and boundary conditions everywhere (formation of the matrix A), and then defining the Galerkin matrix taking the scalar product of these evaluations ($A^T A$). As a result, it is not affected by the potential ill-posedness of the weak form, and the resulting linear system is guaranteed to be invertible.

For the first case, we considered equation 1 with $a = 1, \mu = 1$ and imposed a split boundary conditions of Dirichlet and Robin. The degeneration comes from the Robin boundary condition, for which we set

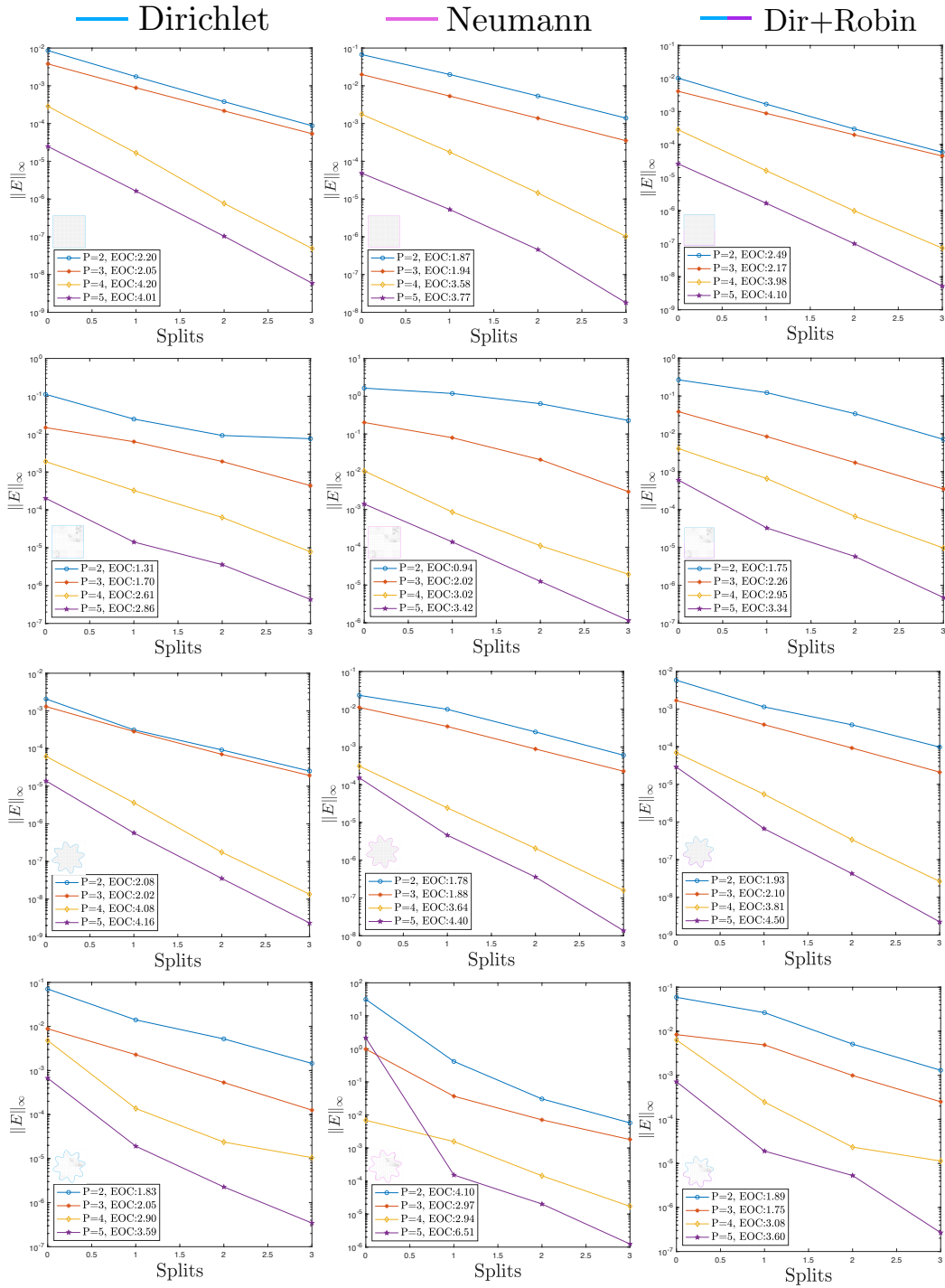


Figure 9: Convergence of L^∞ global error for several configurations. Columns denote boundary condition type. Rows correspond to (1) a uniform grid on a square domain, (2) adaptive square, (3) uniform octofoil, and (4) adaptive octofoil (top to bottom). See Figure 7 for mesh examples.

$\beta = 1, \gamma = -1$. For the second case, we keep $a = 1$, but set $\mu = -100$ (i.e. Helmholtz's equation), and enforce a Dirichlet boundary condition. The convergence results are depicted in Figure 10. The method achieves h-P convergence for both of the degenerate cases and all grid configurations. The numerical

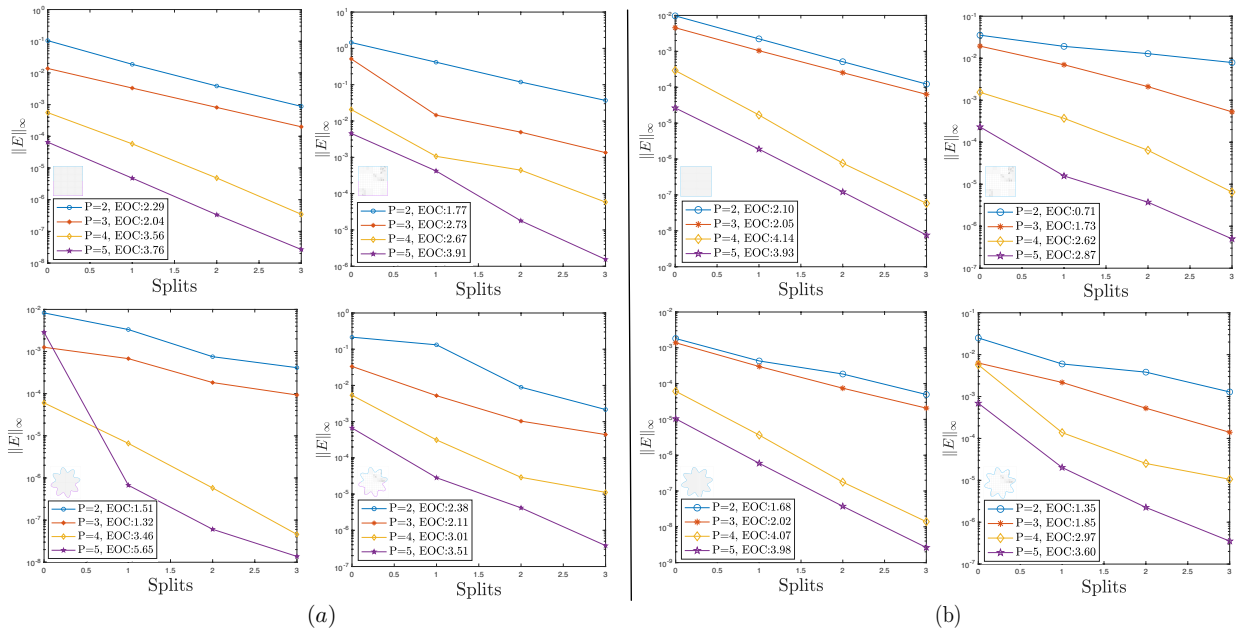


Figure 10: Two instances of a degenerate case: (a) Mixed Robin and Dirichlet boundary conditions, (b) Dirichlet boundary condition for a highly negative value of μ .

error dips rapidly below reasonable error tolerances, and the EOC behaves normally, increasing with the polynomial order and split number. We note that results using exclusively traditional Robin boundary conditions ($\beta = 1$, $\gamma = 1$) on the entire domain achieved the similar results.

4.4. Sensitivity to Problem Parameters

Despite consistent patterns of convergence for various boundary conditions tested here (*i.e.* dirichlet, dirichlet + robin, degenerate, *etc.*), Neumann boundary conditions seem to perform poorly – especially on adaptive grids. In fact, in Figure 9, we observe errors of magnitude upwards of 10^1 and even 10^2 .

From (1), we note that when μ is significantly smaller than a , the problem resembles an interpolation problem, which is relatively straightforward to solve. On the other hand, if a is considerably smaller than μ , the equation resembles a – potentially – ill-posed Poisson problem, *e.g.* failing the solution uniqueness criterion. In fact, the well-posedness of the Poisson problem under Neumann boundary conditions hinges on factors such as the smoothness of the domain and boundary, the characteristics of the Neumann boundary data g , and how well the boundary conditions align with the given problem. When the Neumann boundary condition fails to offer sufficient information to determine u uniquely, it can result in non-uniqueness or instability within the solution, rendering the problem ill-posed. Therefore, by setting $a = \mu = 1$, the well-posedness of the problem could have impacted the convergence/accuracy in the Neumann boundary condition setting. To investigate this, we select four different values of $\frac{a}{\mu}$. The expectation is that as we increase the ratio, the problem should become easier to solve.

Presented in Figure 11 (a) are convergence results for Neumann boundary conditions imposed on the octofoil interface with a uniform grid for $\frac{a}{\mu} = 1, 10, 100, 1000$. We observe that for each polynomial basis order, P , the global error maintains a similar trend among the four tested ratios $\frac{a}{\mu}$, respectively. This behavior corroborates the congruity of the Estimated Order of Convergence (EOC) between various $\frac{a}{\mu}$ given order P . Clearly, the method performs as expected with the Neumann constraint across the various ratios; nonetheless, it is noteworthy that larger values of $\frac{a}{\mu}$ allow for a significant decrease in the global error (≈ 2 orders of magnitude). In fact, when $\frac{a}{\mu} \geq 100$, the method demonstrates accuracy comparable to, or surpassing, that which was achieved with Dirichlet boundary conditions. Hence, with Neumann boundary conditions, smaller values of $\frac{a}{\mu}$ can compromise the effectiveness of the method.

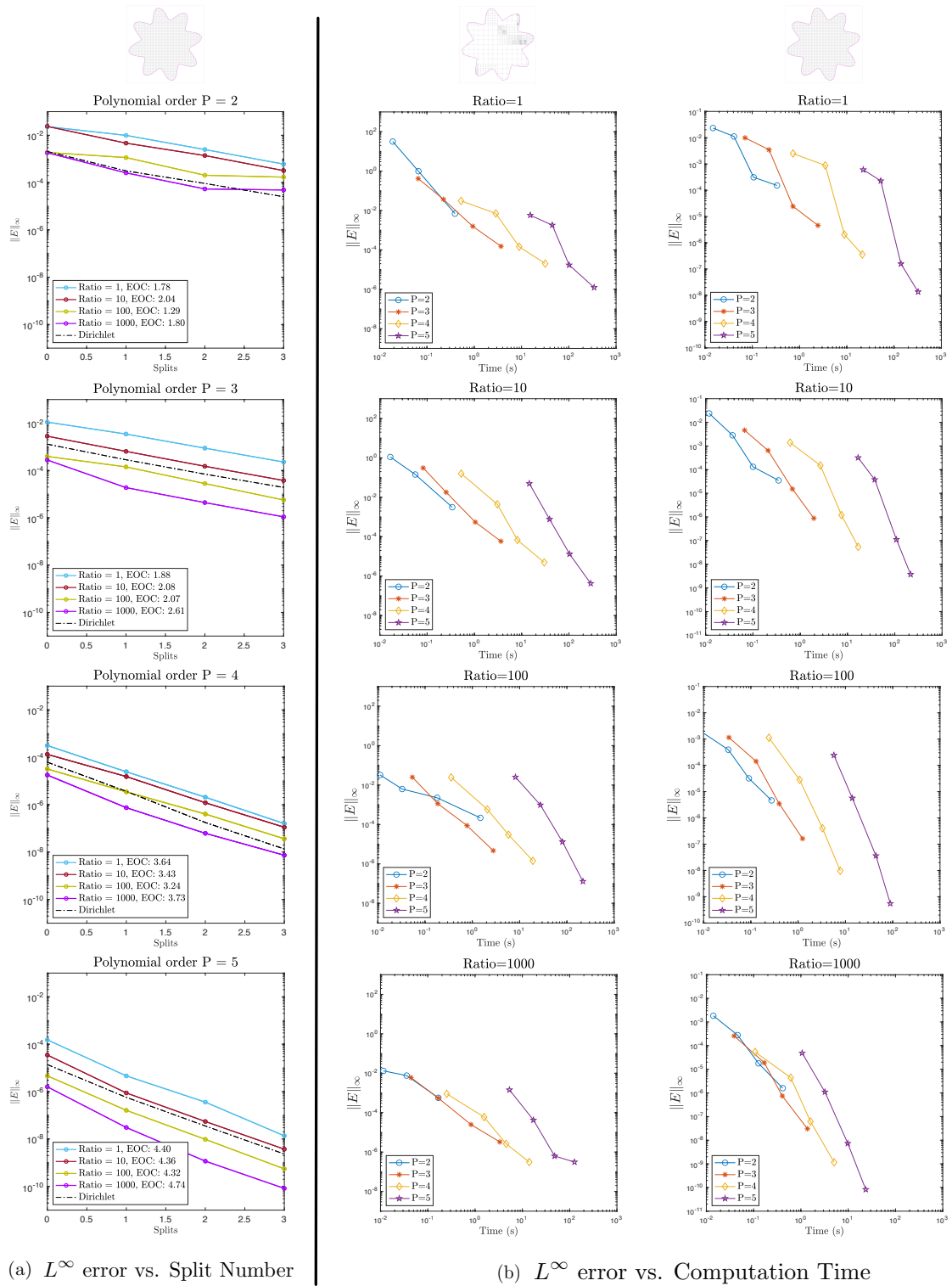


Figure 11: Neumann boundary condition on the octofoil domain: impact of $\frac{\alpha}{\mu}$ ratios. (a) Global error trend for increasing split number for a uniform grid for each polynomial basis. (b) Impact of computational time on global error for both adaptive and uniform grid types.

4.5. Computational Time

Previously, it was established that lower $\frac{\alpha}{\mu}$ ratio values associated with a Neumann boundary condition create a more challenging computational problem (4.4). For this reason, we showcase the performance and efficiency of the LSQD method by exploring a variety of $\frac{\alpha}{\mu}$ ratios. Figure 11 (b) illustrates the maximum error obtained by our solver in comparison to the time it took to run in serial on a Dell precision 3240. It is apparent that, in general, achieving a lower maximum error requires a longer runtime and higher polynomial order. However, we also see that as the ratio $\frac{\alpha}{\mu}$ decreases, not only does it take more time to solve the system, but the order of accuracy declines.

We also note that the slope of the error versus computational times increases with the polynomial order, suggesting that in the asymptotic limit of highly resolved simulations (small error or large CPU time), high-polynomial computations will always be the most efficient. Though, for the presented results this asymptotic regime is never reached. Therefore, in practice, it is imperative to decide which variable (minimizing error or computational cost) takes precedence in a given setting. Presuming that the modeled system has a tight tolerance for error, while computational resources are not a primary concern, the conspicuous objective is achieving a low global error. Figure 11(b) hints at the necessary setup for attaining specific accuracy levels; the higher the polynomial basis order, the higher the accuracy. However, if the priority shifts towards saving computational time and/or memory or simply capturing the general behavior of the solution, opting for a moderately compact setup and a lower-order polynomial basis might suffice.

4.6. Error Estimator

We propose an alternative way to compute local error estimate as:

$$\|e_u(\tilde{\mathbf{x}})\|_{Est} = \max \left| \sum_{q=1}^Q \alpha_{l_1}^q \phi_{l_1}^q(\tilde{\mathbf{x}}) - \sum_{q=1}^Q \alpha_{l_2}^q \phi_{l_2}^q(\tilde{\mathbf{x}}) \right|, \quad l_1, l_2 \in L = (\text{neighboring cells}). \quad (24)$$

Obtaining analytical solutions to PDEs is only possible in the simplest cases, so it should be expected that the exact solution to the PDE (1) may not be available. This error estimator is built into the algorithm, as evaluating accuracy predicated on traditional methods tends to be infeasible. For a comparison between the theoretical prediction and practical results, we restrict our analysis to the Dirichlet case.

The function of our node-based error estimator is to compare local approximations from neighboring cells. All corners of the cells located inside the domain become node locations $\tilde{\mathbf{x}}_i$. For each node, the touching cells are used to calculate the error. In one dimension, we can picture the error as the discontinuity between two local expansions around that node (see Figure 2). To visualize this process in two dimensional space, refer once again to Figure 12(a). If we want to compute the estimate error around the reference node (in blue), we use the local approximation functions constructed for the closest neighbor cells (black), and evaluate at the considered reference node $\tilde{\mathbf{x}}_i$ (note that the maximum amount of neighboring cells is four: left, right, top, and bottom). Finally, the error estimate is computed as the maximum difference between the local values obtained.

Focusing, in particular, on Figure 12(b-c), we are able to see a comparison between simulation error and estimated error for multiple polynomial orders and for increasing grid refinement. These results are encapsulated, numerically, in 12(b), where calculations (on legend) generalize that the predicted EOC is consistently higher than the actual EOC. However, when taking a closer look at the distribution of the colored (simulated) and dashed lines (predicted), the predicted global error is not free of variance, meaning that neither the simulated, nor the predicted global error is consistently superior. It becomes evident (see fig. 12(c)) that the main differences between our actual and estimated error are transpiring at the boundary of our octofoil domain. Nonetheless, the most stark differences dissipate as the grid is refined (this is referred to as ‘Splits’). Overall, we find that this cheap built-in estimator offers meaningful global error and convergence estimates.

5. Discussion / Conclusion

In this paper, we proposed a new paradigm for solving elliptic PDEs, one that would retain all of the advantages of meshless methods, while remaining accessible in theory and in practice. Least Squares

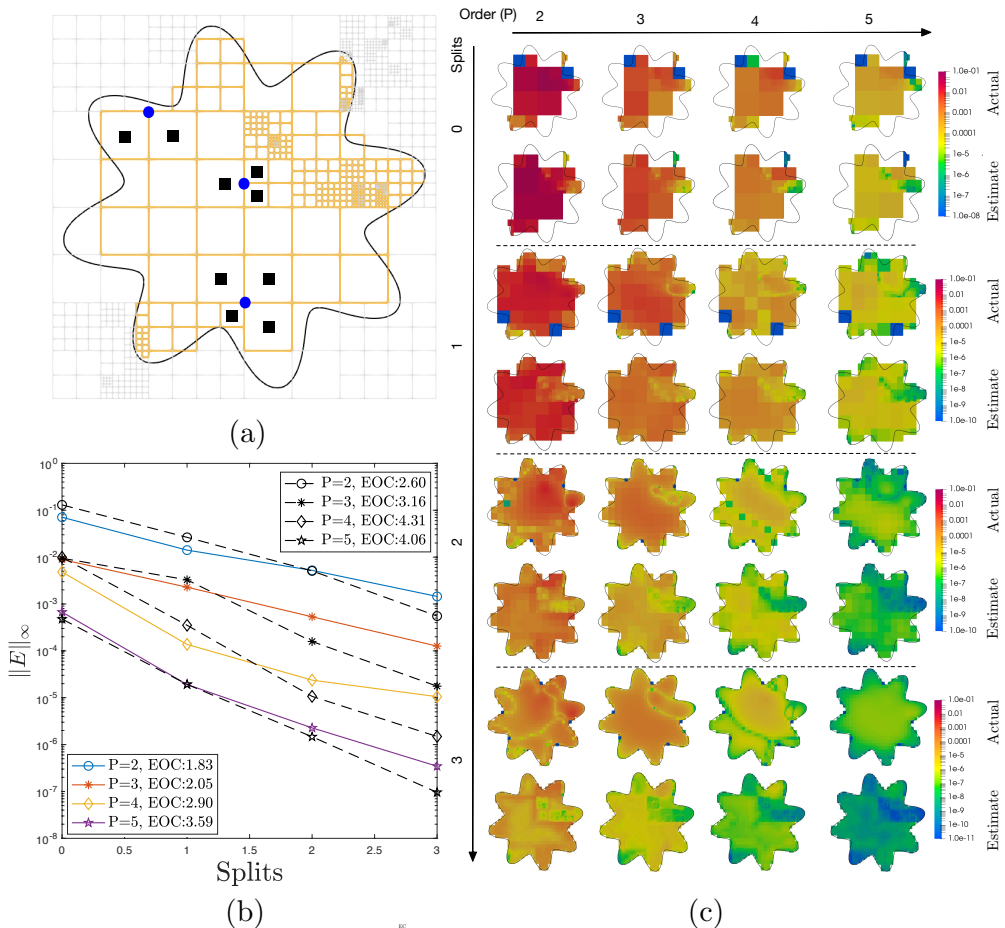


Figure 12: Error Estimator Analysis on adaptive grids: (a) Three distinct node locations and what is considered their respective surrounding/neighbors cells. (b) Comparison between computational order of accuracy (colored lines) and predicted order of accuracy (dashed lines). (c) Illustration of computational and predicted error for increasing polynomial order and grid refinement.

Discretization Method (LSQD) does not require any quadrature rules, weak formulations, body-fitted grids, nor does it necessitate advanced mathematical theory. Nevertheless, it constructs h-P converging numerical solutions on non-trivial data structures with reasonable computational complexity. LSQD method easily handles complex geometries and is virtually impervious to ill-posed problems.

Although we began with a one-dimensional proof of concept, we demonstrated the feasibility in extending our method to a higher dimensional space, and its applicability to a broad range of problems, boundary conditions, and computational parameters (*e.g.* grid resolution, polynomial orders). For all considered cases, we consistently observe h-P convergence, with Estimated Order of Convergence (EOC) ranging from 1.83 to 4.53 (see Table 1), and in practice the global error falls rapidly below any reasonable error tolerance. Moreover, when investigating degenerate cases (*i.e.* where the problem is potentially ill-posed as a consequence of the PDE coefficients or boundary conditions), the method observes kindred results (see 4.3), exemplifying the robustness of the LSQD method.

Finally, we proposed an *a posteriori* node-based error estimator to unveil the local solution agreement. From Fig 12 (c), we see that as the polynomial order increases and the grid is refined, the estimated and measured/experimental errors display the same convergence pattern and similar spatial localization. This estimator cannot be used as a lower bound for actual error as seen in 12(c), but provides a general blueprint for where error is to be expected and, thus, can be used for optimal mesh refinement. Coupled with a spatial adaptivity capability, this error estimator could be used as an error controller.

From our computational time analysis (see 4.5), we observed steeper efficiency curves for higher polynomial orders, suggesting that using high-order representations might be advantageous, at least for very large systems. In practice, for small test problems like the ones considered here, these benefits may not manifest, and low polynomial orders seem to be the best strategy to get an accurate solution rapidly. In the examples presented here, computational times peaked around 10^3 seconds on a single core, or ≈ 17 minutes for the largest systems ($\approx 1.3 \times 10^6$ degrees of freedom for 4 splits and $P=5$). Even though we are willing to sacrifice computational time for ease of implementation, these values are significant and suggest that the method must be optimized to be of full practical interest.

In this case, we have two avenues for optimization, either we can prioritize reducing the CPU time or the numerical error. Since most of the computational time is dedicated to solving the least square system, accelerating the method would entail speeding up the linear solver and ultimately reducing the condition number. The method offers a number of free parameters and tuning knobs, such as the positions of the evaluation points, the number of neighbors, the basis functions selection, or the possibility to weight equations differently in the overdetermined system. We believe the method can be optimized by investigating the impact of these parameters on the accuracy of the solution and conditioning of the system.

Despite our presentation and analysis being restricted to low-dimensional examples and an un-optimized approach, we see that the LSQD method is a robust and versatile tool for computational scientists. Its minimal theoretical and programming barriers render it accessible to a broad scientific community, and we anticipate that further research endeavors could propel it into a formidable simulation paradigm.

6. Acknowledgments

The authors thank Arnold Kim for valuable discussions. This material is based upon work supported by the National Science Foundation under Grant No. DMS-1840265.

Credit author statement

Anna Kucherova: Investigation, Formal Analysis, Software, Visualization, Writing - Original Draft, Writing - Review & Editing. **Gbocho Terasaki:** Formal Analysis, Investigation, Software, Visualization, Writing - Original Draft, Writing - Review & Editing. **Selma Strango:** Preliminary Investigation, Formal Analysis, Software, Writing - Review & Editing. **Maxime Theillard:** Conceptualization, Supervision, Formal Analysis, Methodology, Software, Project Administration, Writing - Original Draft, Writing - Review & Editing.

References

- [1] S. N. Atluri and T. Zhu. A new meshless local petrov-galerkin (mlpg) approach in computational mechanics. *Computational Mechanics*, 22(2):117–127, Aug 1998.
- [2] S. N. Atluri and T.-L. Zhu. The meshless local petrov-galerkin (mlpg) approach for solving problems in elasto-statics. *Computational Mechanics*, 25(2):169–179, Mar 2000.
- [3] I. Babuska and J. M. Melenk. The partition of unity method. *International Journal for Numerical Methods in Engineering*, 40(4):727–758, 1997.
- [4] T. Belytschko, Y. Krongauz, D. Organ, M. Fleming, and P. Krysl. Meshless methods: An overview and recent developments. *Computer Methods in Applied Mechanics and Engineering*, 139(1):3 – 47, 1996.
- [5] T. Belytschko, Y. Y. Lu, and L. Gu. Element-free galerkin methods. *International Journal for Numerical Methods in Engineering*, 37(2):229–256, 1994.
- [6] T. Belytschko, D. Organ, and C. Gerlach. Element-free galerkin methods for dynamic fracture in concrete. *Computer Methods in Applied Mechanics and Engineering*, 187(3):385 – 399, 2000.
- [7] M. Blomquist, S. R. West, A. L. Binswanger, and M. Theillard. Stable nodal projection method on octree grids. *Journal of Computational Physics*, 499:112695, 2024.
- [8] K. C. Chung. A generalized finite-difference method for heat transfer problems of irregular geometries. *Numerical Heat Transfer*, 4(3):345–357, 1981.
- [9] P. C. Curtis. n -parameter families and best approximation. *Pacific J. Math.*, 9(4):1013–1027, 1959.
- [10] Q. Du, M. D. Gunzburger, and L. Ju. Voronoi-based finite volume methods, optimal voronoi meshes, and pdes on the sphere. *Computer Methods in Applied Mechanics and Engineering*, 192(35):3933 – 3957, 2003.
- [11] Y. Duan. A note on the meshless method using radial basis functions. *Computers & Mathematics with Applications*, 55(1):66–75, 2008.
- [12] C. A. Duarte and J. T. Oden. H-p clouds—an h-p meshless method. *Numerical Methods for Partial Differential Equations*, 12(6):673–705, 1996.
- [13] A. Eirís, L. Ramírez, I. Couceiro, J. Fernández-Fidalgo, J. París, and X. Nogueira. Mls-sph-ale: A review of meshless-fv methods and a unifying formulation for particle discretizations. *Archives of Computational Methods in Engineering*, 30(8):4959–4981, 2023.
- [14] B. Fornberg and N. Flyer. Solving pdes with radial basis functions. *Acta Numerica*, 24:215–258, 2015.
- [15] R. Franke. Scattered data interpolation: tests of some methods. *Mathematics of Computation*, 38:181–200, 1982.
- [16] E. J. Fuselier and G. B. Wright. A high-order kernel method for diffusion and reaction-diffusion equations on surfaces. *Journal of Scientific Computing*, 56:535–565, 2013.
- [17] C. Fylling, J. Tamayo, A. Gopinath, and M. Theillard. Multi-population dissolution in confined active fluids. *Soft Matter*, 20:1392–1409, 2024.
- [18] R. A. Gingold and J. J. Monaghan. Smoothed particle hydrodynamics: theory and application to non-spherical stars. *Monthly Notices of the Royal Astronomical Society*, 181(3):375–389, 12 1977.
- [19] D. González, E. Cueto, and M. Doblaré. *Towards an Isogeometric Meshless Natural Element Method*. Springer Netherlands, Dordrecht, 2009.
- [20] A. Guittet, M. Theillard, and F. Gibou. A stable projection method for the incompressible navier-stokes equations on arbitrary geometries and adaptive quad/octrees. *J. Comput. Phys.*, 292:215–238, 2015.
- [21] R. L. Hardy. Multiquadric equations of topography and other irregular surfaces. *Journal of Geophysical Research (1896-1977)*, 76(8):1905–1915, 1971.
- [22] B. He, J. Li, M. Chen, and Y. Huang. A leap-frog meshless method with radial basis functions for simulating electromagnetic wave splitter and rotator. *Engineering Analysis with Boundary Elements*, 118:225–242, 2020.
- [23] A. A. Heydari, S. S. Sindi, and M. Theillard. Conservative finite volume method on deforming geometries: The case of protein aggregation in dividing yeast cells. *Journal of Computational Physics*, 448:110755, 2022.
- [24] B.-n. Jiang. *Basis of LSFEM*, pages 47–79. Springer Berlin Heidelberg, Berlin, Heidelberg, 1998.
- [25] B.-N. Jiang and L. A. Povinelli. Least-squares finite element method for fluid dynamics. *Computer Methods in Applied Mechanics and Engineering*, 81(1):13–37, 1990.
- [26] G. Joldes, G. Bourantas, B. Zwick, H. Chowdhury, A. Wittek, S. Agrawal, K. Mountris, D. Hyde, S. K. Warfield, and K. Miller. Suite of meshless algorithms for accurate computation of soft tissue deformation for surgical simulation. *Medical Image Analysis*, 56:152–171, 2019.
- [27] E. Kansa. Multiquadrics—a scattered data approximation scheme with applications to computational fluid-dynamics—ii solutions to parabolic, hyperbolic and elliptic partial differential equations. *Computers Mathematics with Applications*, 19(8):147 – 161, 1990.
- [28] E. Kansa and Y. Hon. Circumventing the ill-conditioning problem with multiquadric radial basis functions: Applications to elliptic partial differential equations. *Computers & Mathematics with Applications*, 39(7):123–137, 2000.
- [29] I. Kovacevic, A. Poredos, and B. Sarler. Solving the stefan problem with the radial basis function collocation method. *Numerical Heat Transfer: Part B: Fundamentals*, 44:575–599, 12 2003.
- [30] A. Kucherova, S. Strango, S. Sukenik, and M. Theillard. Computational modeling of protein conformational changes - application to the opening sars-cov-2 spike. *Journal of Computational Physics*, 444:110591, 2021.
- [31] M. Kumar, A. K. Jha, Y. Bhagoria, and P. Gupta. A review to explore different meshless methods in various structural problems. *IOP Conference Series: Materials Science and Engineering*, 1116(1):012119, apr 2021.
- [32] S. Kumar, K. Danas, and D. M. Kochmann. Enhanced local maximum-entropy approximation for stable meshfree simulations. *Computer Methods in Applied Mechanics and Engineering*, 344:858–886, 2019.
- [33] T. Liszka and J. Orkisz. The finite difference method at arbitrary irregular grids and its application in applied mechanics. *Computers & Structures*, 11(1):83 – 95, 1980. Special Issue-Computational Methods in Nonlinear Mechanics.

- [34] W. K. Liu, S. Jun, and Y. F. Zhang. Reproducing kernel particle methods. *International Journal for Numerical Methods in Fluids*, 20(8-9):1081–1106, 1995.
- [35] L. B. Lucy. A numerical approach to the testing of the fission hypothesis. 82:1013–1024, 1977.
- [36] N. Mai-Duy and T. Tran-Cong. Numerical solution of navier–stokes equations using multiquadric radial basis function networks. *International Journal for Numerical Methods in Fluids*, 37(1):65–86, 2001.
- [37] N. Mai-Duy and T. Tran-Cong. Mesh-free radial basis function network methods with domain decomposition for approximation of functions and numerical solution of poisson’s equations. *Engineering Analysis with Boundary Elements*, 26(2):133 – 156, 2002.
- [38] J. C. Mairhuber. On haar’s theorem concerning chebychev approximation problems having unique solutions. *Proceedings of the American Mathematical Society*, 7(4):609–615, 1956.
- [39] F. Mazhar, A. Javed, J. T. Xing, A. Shahzad, M. Mansoor, A. Maqsood, S. I. A. Shah, and K. Asim. On the meshfree particle methods for fluid-structure interaction problems. *Engineering Analysis with Boundary Elements*, 124:14–40, 2021.
- [40] C. A. Micchelli. Interpolation of scattered data: Distance matrices and conditionally positive definite functions. *Constructive Approximation*, 2(1):11–22, 1986.
- [41] V. P. Nguyen, T. Rabczuk, S. Bordas, and M. Duflot. Meshless methods: A review and computer implementation aspects. *Mathematics and Computers in Simulation*, 79(3):763–813, 2008.
- [42] E. Onate, S. Idelsohn, O. C. Zienkiwicz, and R. L. TAYLOR. A finite point method in computational mechanics. applications to convective transport and fluid flow. *International Journal for Numerical Methods in Engineering*, 39(22):3839–3866, 1996.
- [43] C. C. Paige and M. A. Saunders. Lsqr: An algorithm for sparse linear equations and sparse least squares. *ACM Trans. Math. Softw.*, 8(1):43–71, Mar. 1982.
- [44] V. G. Patel and N. V. Rachchh. Meshless method – review on recent developments. *Materials Today: Proceedings*, 26:1598–1603, 2020. 10th International Conference of Materials Processing and Characterization.
- [45] C. Piret. The orthogonal gradients method: A radial basis functions method for solving partial differential equations on arbitrary surfaces. *Journal of Computational Physics*, 231(14):4662 – 4675, 2012.
- [46] M. J. Powell. Five lectures on radial basis functions. Technical report, Informatics and Mathematical Modelling, Technical University of Denmark, DTU, Richard Petersens Plads, Building 321, DK-2800 Kgs. Lyngby, 2005.
- [47] H. Samet. An overview of quadtrees, octrees, and related hierarchical data structures. 1988.
- [48] B. Sarler. A radial basis function collocation approach in computational fluid dynamics. *Computer Modeling in Engineering & Sciences*, 7(2):185–194, 2005.
- [49] B. Sarler, J. Perko, and C.-S. Chen. Radial basis function collocation method solution of natural convection in porous media. *International Journal of Numerical Methods for Heat & Fluid Flow*, 14:187–212, 03 2004.
- [50] B. Sarler and R. Vertnik. Meshfree explicit local radial basis function collocation method for diffusion problems. *Computers Mathematics with Applications*, 51(8):1269 – 1282, 2006. Radial Basis Functions and Related Multivariate Meshfree Approximation Methods: Theory and Applications.
- [51] M. A. Saunders. Solution of sparse rectangular systems using lsqr and craig. *BIT Numerical Mathematics*, 35(4):588–604, 1995.
- [52] C. Shu, H. Ding, H. Chen, and T. Wang. An upwind local rbf-dq method for simulation of inviscid compressible flows. *Computer Methods in Applied Mechanics and Engineering*, 194(18):2001 – 2017, 2005.
- [53] S. Soleimani, M. Jalaal, H. Bararnia, E. Ghasemi, D. Ganji, and F. Mohammadi. Local rbf-dq method for two-dimensional transient heat conduction problems. *International Communications in Heat and Mass Transfer*, 37(9):1411 – 1418, 2010.
- [54] N. Sukumar, B. Moran, and T. Belytschko. The natural element method in solid mechanics. *International Journal for Numerical Methods in Engineering*, 43(5):839–887, 1998.
- [55] G. B. Wright, N. Flyer, and D. A. Yuen. A hybrid radial basis function–pseudospectral method for thermal convection in a 3-d spherical shell. *Geochemistry, Geophysics, Geosystems*, 11(7), 2010.
- [56] J. Yvonnet, D. Ryckelynck, P. Lorong, and F. Chinesta. A new extension of the natural element method for non-convex and discontinuous problems: the constrained natural element method (c-nem). *International Journal for Numerical Methods in Engineering*, 60(8):1451–1474, 2004.
- [57] T. Zhu, J.-D. Zhang, and S. N. Atluri. A local boundary integral equation (lbie) method in computational mechanics, and a meshless discretization approach. *Computational Mechanics*, 21(3):223–235, Apr 1998.